Journal of Intelligent Systems and Internet of Things
Vol. 18, No. 01, PP. 288-297, 2026
DOI: https://doi.org/10.54216/JISIoT.180122

Machine Learning Model Based Urban Temperature Analysis with Fuzzy Reinforcement Neural Network

L. Pallavi[1,*], Gattu Shravani[2], J. Sirisha Devi[3], Bandaru Satya Lakshmi[4], M. Pushpalatha[5], S. Gopinath[6], M. Rajesh[7]

[1]Associate Professor, Department of Computer Science and Engineering, B V Raju Institute of Technology, Narsapur, Telangana, India

[2]Assistant Professor, Dept of CSE (Cys, DS, AI&DS), VNRVJIET, Bachupally, Hyderabad Telangana -500090, India

[3]Professor, Department of Computer Science and Engineering, Koneru Lakshmaiah Education Foundation, Bowrampet, Hyderabad 500043, Telangana, India

[4]Assistant Professor, Computer Science and Engineering, Aditya University, Surampalem, Andhra Pradesh, India

[5]Assistant Professor, Department of Computer science and Technology, Karpagam College of Engineering, Tamil Nadu, India

[6]Assistant Professor, Gnanamani College of Technology, Namakkal, Tamilnadu-637018, India

[7]Department of Computer Science and Engineering, Aarupadai Veedu Institute of Technology, Vinayaka Mission's Research Foundation (DU), Tamilnadu, India

Emails: pallavi503@gmail.com; gattushravani513@gmail.com; Siri.cse21@gmail.com; satyalakshmi91.bandaru@gmail.com; pushpalatha18494@gmail.com; sgopicse@gmail.com; rajesmano@gmail.com

Abstract

Temperature increases in metropolitan areas are referred to as urban heat island (UHI) effect. In recent decades, urbanization as well as dramatic increase in population of cities have exacerbated the impact of UHI. The uneven development and growth of the metropolis will lead to an uneven rate of temperature growth in the corresponding area. This work proposes a new machine learning approach based on temperature pattern analysis to determine the rate of deforestation, representing the diversity of geographical regions. The proposed model collect temperature pattern based deforestation data as well as processed for noise removal and normalization. Then this data features has been extracted as well as classified utilizing kernel principal fuzzy reinforcement NN with variational Gaussian encoder markov model. Experimental analysis is carried out in terms of random accuracy, mean precision, AUC, normalized co-efficient, F1 score. Proposed method mean precision was 94%, normalized co-efficient was 97%, AUC was 95%, random accuracy 98%, F1-score 93%. The most important land use categories causing LST increases were determined by analyzing the landscape composition at the class level.

Received: March 19, 2025 Revised: June 08, 2025 Accepted: July 13, 2025

Keywords: Urban heat island; Encoder markov model; Fuzzy reinforcement; Geographical region diversity; Gaussian encoder

1. Introduction

In addition to being extremely vulnerable, tropical dry forests are also very important ecologically. However, the effects of their disappearance in context of climate change have not received much attention. Because trees can absorb solar radiation and refract it, forests provide options for surface cooling. Based on biophysical factors, forests can have a significant impact on the local land surface temperature since they typically have higher evapotranspiration and a lower surface albedo than non-forested places. However, if forests are not maintained appropriately and sustainably, these environmental benefits may be diminished or even eliminated. Temperature extremes can be greatly influenced by changes in land use [1]. In fact, deforestation processes directly impact physical features of land surface, and these changes have potential to significantly affect fluxes of heat, carbon, moisture in atmospheric circulation as well as climate. Extreme weather events and changes in the land surface are causing variations in Land Surface Temperature (LST) distributions throughout different biomes globally. Removing forest cover increases absorption of solar shortwave radiation, which increases wind chill and releases longwave radiation within a few hours [2]. Deforestation somewhat raises albedo and greatly lowers evapotranspiration in tropical regions, which warms the planet's temperature. Additionally, the loss of forests results in cooling during the night and warming during the day. A significant increase in LST levels is also being caused by changes in land use brought about by expansion of urban, periurban, rural areas. Urbanization processes change albedo, increase impervious surfaces, decrease natural vegetation, and increase the risk of heat stress for urban populations compared to rural ones. This phenomenon is known as "Urban Heat Island" [3]. Note that a sizable portion of the hilly northern region ravaged by the flash floods is missing from this image, which solely depicts flooded plain areas. The nation's catastrophe response and recovery efforts faced enormous hurdles because of extreme weather phenomena like cloud bursts and unusual rains, which caused extensive harm. The nation's vital infrastructure and human lives suffered greatly because of the floods. There have been instances of trees being carried away by floodwaters during flooding, particularly in country's northern regions. Reforestation efforts have been severely hampered by the fact that many of these trees were planted as part of government's Billion Tree Tsunami campaign in recent years.

Comprehensive examination of land use as well as land cover is greatly enhanced by use of satellite photography as well as remote sensing. These cutting-edge technologies offer a thorough perspective of landscapes, vegetation, water bodies, metropolitan areas, providing insightful information about the dynamics of Earth's surface. Furthermore, exact identification of vegetation health, land degradation, deforestation detection are made possible by remote sensing. Several spectral indices, including Soil-Adjusted Vegetation Index (SAVI), Normalized Difference Water Index (NDWI), Normalized Difference Vegetation Index (NDVI), are used to accomplish this [4]. By using machine-learning algorithms, land use classification becomes even more accurate and efficient, enabling evidence-based decision-making for conservation as well as sustainable land management. With advancement of remote sensing methods, detection of deforestation and land use applications are becoming increasingly important in tackling current environmental concerns and paving the way for a more resilient future [5].

Research Contribution: to suggest a unique method for detecting the rate of deforestation using machine learning and temperature pattern analysis for modelling geographical region diversity. The suggested model gathers deforestation data based on temperature patterns and processes it for noise reduction and normalization. Then, using a variational Gaussian encoder markov model and a kernel principal fuzzy reinforcement neural network, the features of the data were retrieved and identified.

2. Literature survey

The effectiveness of remote sensing photos as a source of data for forest management has been shown in a number of studies. ML techniques are applied to processing of satellite photos of forests. A computer that has been algorithmically educated to carry out a task, such event prediction or picture classification, is called a machine learning system. Machine learning offers several advantages over traditional statistical techniques, including scalability and flexibility. This allows it to be applied to a wide range of tasks, including categorization, predictions, and the stratification/clustering of phenomena. A machine learning approach was presented in work [6] to improve estimations of the type of forestland cover and metrics related to forest structure. This multitask model combines multiple separate tasks and models into a single stream by doing both classification and regression simultaneously. Author [7] to identify changes in land usage in the Amazon used a machine-learning algorithm. They might distinguish between fires in primary forests and fires in previously burnt regions, which would enhance the present fire scar mapping process and help identify areas at high risk of burning based on change interpretation. A project to identify daily deforestation in the Amazon jungle was suggested by Work [8]. They created a method for using satellite photos to train machine-learning models and carried out a spectrum temporal analysis of the deforestation area. The method made it easier to

comprehend the dynamics of the Amazon rainforest's deforestation. To forecast the possible amount and spatial distribution of Amazonian deforestation, put forth a spatially explicit model of deforestation. The model was verified and spatially deforestation accumulation areas were discovered over time. Author [9] mapped landslip images obtained with extremely high-resolution photographs using object-oriented analysis and the random forest technique. For four test sites, they were able to attain accuracy of between 73% and 87%. A software framework called imageRF was developed by Work [10] to analyses remotely sensed images utilizing random forest technique. Machine learning regression models are also useful for forecasting changes in land use or cover based on historical data sets. Numerous studies have been conducted in this field. By [11], a regression model was developed and applied to evaluate air pollution exposure. The level of deforestation in Amazon rain forest region has been predicted by author [12] using the Bayesian network approach. Additionally, they have referenced Amazon forest data set. They are able to anticipate next Amazonian location to experience deforestation with an accuracy of 90%. The authors [13], proposed the encoder and decoder structures make up the suggested U-Net architecture. The encoder extracts hierarchical data from input images using down sampling and convolutional layers. Context acquisition is aided by every down sample step's reduction of spatial dimensions as well as enhancement of feature depth.

3. Proposed temperature pattern analysis based deforestation rate detection

The global geographical spread and diversity of environmental conditions of these 20 locales make their selection noteworthy. A different geographical and climate zone was represented by each city that was selected. Because of this diversity, we can perform a thorough examination of trends and patterns in global temperature, which advances our knowledge of the dynamics of urban temperature as shown in Figure 1. These cities are located in Europe, Asia, Africa, North and South America, Oceania. Temperature information is taken from WeatherSpark, a website that offers comprehensive weather reports for almost 100,000 locations across the globe. In passing, a temporal index, represented by the symbol t, is applied, and it is used to indicate year of registration for temperature and deforestation data. Two spatial indices are also used, one for the municipality m as well as other for city c. Total size of the input data Xtm has the format $t\times m\times c$t×m×c. The sum of the city index (c) and temporal index (t) yields $t\times c$t×c rows, which is the number of rows. Along with additional columns for city names, mean temperatures ($Tcitymean$Tmeancity), minimum temperatures ($Tcitein$Tmincity), maximum temperatures ($Tcitymbx$Tmaxcity) are also included in the number of municipalities (m=297m=297). The data on deforestation is sourced from TerraBrasilis, an environmental monitoring platform designed for organizing, accessing, and utilizing geographic data. National Institute for Space Research (INPE), a research division of Brazilian Ministry of Science and Technology, TerraBasilis.

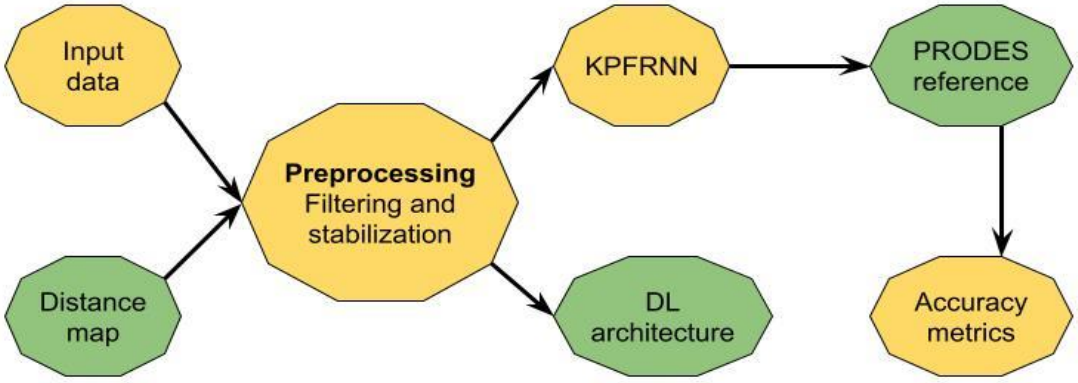

Figure 1. Proposed model in temperature pattern analysis based deforestation rate detection

4. SAR Image Despeckling

One common approach for processing SAR data is speckle reduction. It seeks to improve radar picture interpretation by increasing the signal-to-noise ratio. In this study, we utilised a conventional despeckling method that involves the sequential application of two filters: a temporal filter and a spatial filter. Using a series of previously coregistered images as a guide, we first apply temporal filter to a specific SAR image. Next, we compute the following expression to get the filtered result by eqn (1)

$$J_k = \frac{\hat{\sigma}_k}{M}\sum_{i=1}^{M} \frac{I_t}{\hat{\sigma}_t}\Big| \quad (1)$$

We utilized a revised Lee filter after applying the temporal filter since it preserved and enhanced the edgy aspects of the input photos. The original Lee filter applies the following formulas on local statistics to minimize noise by eqn (2)

$$J = \langle I\rangle + k(I - \langle I\rangle)$$

$$k = \frac{\mathrm{Var}(I)}{\langle I\rangle^2\sigma_0^2 + \mathrm{Var}(I)}$$

$$\sigma_v = \sqrt{\mathrm{Var}(I)}/\langle I\rangle \quad (2)$$

After that, it reshapes it in accordance with edge orientation, lowering the noise variance and the amount of pixels used in the filtering process. Described temporal as well as spatial filters when combined can substantially reduce noise and improve detection accuracy; however the huge number of images considered in the temporal filter stage results in a significant processing cost. Thus, two distinct filtering treatments—**z**1, which just applies spatial filter, **z**2, which employs entire filtering chain—were created and tested in order to calculate effectiveness and necessity of temporal filtering.

5. Kernel principal fuzzy reinforcement neural network (KPFRNN) with variational Gaussian encoder markov (KPFRNN_VGEM) model

When it comes to adaptively choosing kernel principle components to track fault occurrence in real time, the classic KPCA has several drawbacks. Consequently, the kernel principle for chemical processes is adaptively extracted using a moving window integrating threshold approach in AKPCA. Primary objective of the basic KPCA is to extract whitened main components from high-dimensional feature expanse F by shining upon input data using a nonlinear shine upon D. Equation (3) is used to initialise and preprocess the mapped data.

$$\sum_{i=1}^{L} D(x_i) = 0 \quad (3)$$

To create the high feature expanse, which is represented as = [D(x1),..,D(xL)], the mapping function D( ) will be used to shine upon xi to D(xi). Equation (4) represents the covariance matrix in the feature expanse.

$$C = \frac{1}{L}\sum_{i=1}^{L} D(x_i)D(x_i)^T \quad (4)$$

The covariance matrix's feature space containing the eigenvalue and eigenvectors is examined. V is the eigenvector, while Letis is the eigenvalue. Equation (4) can be used to obtain the relationship. λV=CV where 0, √(Var[fo](I))/⟨I⟩is also described as Eq. (5).

$$CV = \left(\frac{1}{L}\sum_{i=1}^{L} D(x_i)D(x_i)^T\right)V = \frac{1}{L}\sum_{i=1}^{L} \langle D(x_i), V\rangle D(x_i) \quad (5)$$

where $\langle \dots \rangle$ points product, so $\lambda V = CV$ is equal by eqn (6)

$$\lambda\langle D(x_k), V\rangle = \langle D(x_k), CV\rangle, k = 1,2, \dots, L \quad (6)$$

Nonlinear conversion must be achieved in dependence on a kernel function k (xi, xj). Determining a L × L gram kernel matrix K using Eq. (7) as a basis.

$$[K]_{ij} = K_{ij} = \left\langle D(x_i), D\left(x_j\right)\right\rangle \quad (7)$$

If matrix rows and columns are denoted by i, j = 1,2,..., L, is substituted by a leading into a kernel function of the following eqn (8)

$$K(x, y) = \langle F(x), F(y)\rangle \quad (8)$$

Assuming that N measurements of u(k) and y(k), for k = 1, 2,..., N, are collected as part of a training data set under normal operating conditions, the following is how the past and future Hankel matrices, Zp and Yf, are formed from zp(k) and yf (k) for all k ∈ [p + 1, p + M] by eqn (9)

$$\boldsymbol{Z}_p = [\boldsymbol{z}_p(p+1) \quad \boldsymbol{z}_p(p+2) \quad \cdots \quad \boldsymbol{z}_p(p+M)]$$

$$\boldsymbol{Y}_f = [y_f(p+1) \quad y_f(p+2) \quad \cdots \quad y_f(p+M)] \quad (9)$$

where M = N − p − f + 1. It is possible to estimate the sample covariance matrices of the cross-covariance matrix and the past and future vectors by eqn (10)

$$\boldsymbol{\Sigma}_{pp} = \frac{1}{M-1} Z_p \boldsymbol{Z}_p^T$$

$$\boldsymbol{\Sigma}_{\mathrm{II}} = \frac{1}{M-1} \boldsymbol{Y}_f \boldsymbol{Y}_f^T$$

$$\boldsymbol{\Sigma}_{\mathrm{tp}} = \tfrac{1}{M-1} \boldsymbol{Y}_f \boldsymbol{Z}_p^T. \quad (10)$$

A look-up table for storing q values can be used to develop Q learning for small datasets. However, the look-up table-based strategy is ineffective for very big datasets. Therefore, function approximation can be used to estimate the Q function and solve the problem. This study scales up Q learning by using fuzzy logic as a function approximation in place of the Q table. The fuzzy has now been used to approximate Q functions. At instant k, the input state vector is matched via fuzzy Q learning by eqn (11)

$$c^k = \{c_1^l, c_2^l, \ldots, c_n^l\} \quad (11)$$

To generate firing strength, n = is a state variable. R_i:α_i (c^l) represents the potential m discrete action by eqn (12)

$$Q = \{q_1, q_2, \ldots, q_m\} \quad (12)$$

additionally, under the fuzzy inference system (FIS), every rule Ri, i N∈ by a w value that describes the virtue of each action by eqn (13)

R_i: If c_1^l is T_1^i and..... and c_n^l is T_n^i then $q = q_1$ with $w(i,1)$or $q = q_2$ with $w(i,2)$or $q = q_m$ with $w(i,m)$ (13)

The membership function of variable l cx under rule Ri is represented by i Tx α, which is a Gaussian type, where i Tx = linguistic word (target value). where qn=WSn and q1=WS1... For input1, fuzzy set layered over universe of discourse is denoted by value 1 l c. The membership function of Gaussians that is utilized is given by eqn (14)

$$\alpha_{\text{input}}(c_1) = e^{-(c_1 - j_1)^2 / 2\sigma_1^2}$$

$$\log p_\theta(x \mid c) \geq \mathbb{E}_{q_\phi(z|x)} \left[\log p_\theta(x \mid z) - \log \frac{q_\phi(z|x)}{p_\theta(z|c)} \right] \quad (14)$$

Rather than utilizing a raw waveform, as indicated by xmel, we employ a mel-spectrogram as the goal data point in the reconstruction loss. After passing through a decoder to upsample latent variables z to waveform domain yˆ, we transform yˆ into the melspectrogram domain xˆmel. Next, reconstruction loss is determined by utilizing L1 difference between target as well as anticipated mel-spectrogram by eqn (15)

$$L_{\text{recon}} = \| x_{mel} - \hat{x}_{\text{mel}} \|_1 \quad (15)$$

This is known as the maximum likelihood estimate if the data distribution is taken to have a Laplace distribution and constant terms are ignored. Our goal is to provide more high-resolution data for posterior encoder. Consequently, we substitute linear-scale spectrogram of target speech xlin for the mel-spectrogram as input. Note that modified input complies with variational inference rules. This brings us to the KL divergence by eqn (16)

$$L_{kl} = \log q_\phi(z \mid x_{\text{lin}}) - \log p_\theta(z \mid c_{\text{text}}, A)$$

$$z \sim q_\phi(z \mid x_{\text{lin}}) = N\left(z; \mu_\phi(x_{\text{lin}}), \sigma_\phi(x_{\text{lin}})\right) \quad (16)$$

apply a normalizing flow fθ on top of factorized normal prior distribution, allowing an invertible transformation of a basic distribution into a more complicated distribution by following the change-of-variables rule by eqn (17)

$$p_\theta(z \mid c) = N(f_\theta(z); \mu_\theta(c), \sigma_\theta(c)) \left| \det \frac{\partial f_\theta(z)}{\partial z} \right|$$

$$c = [c_{\text{text}}, A] \quad (17)$$

The ELBO regularizes posterior distribution qφ(z|x) to fit a preset prior p(z) and minimizes the reconstruction error of the model through the probability of the data given a latent log p□(x|z). Neural networks named encoder and decoder, respectively, parametrize both posterior distributions, qφ and p□ by eqn (18)

$$\dot{\mathbf{s}}(x) = \mathbf{F}\mathbf{s}(x) + \mathbf{L}\varepsilon(x),\ f(x) = \mathbf{H}\mathbf{s}(x) \qquad (18)$$

where the emission, noise effect, and feedback matrices are represented by F ∈ R d×d, L ∈ R d×e, and H ∈ R 1×d, respectively. Most widely-used GP kernels permit the above form (on one-dimensional inputs). The expression p(f(·)| y) = R p(f(·),f | y) df = R p(f(·)|f) p(f | y) df represents the actual posterior process. Here, all potential function evaluations (including u and f) are indicated by the notation f(·). This formula uses function evaluations f = f(X) to capture data flow from data y. An approximate posterior process of type is constructed using sparse approximations by eqn (19)

$$q(f(\cdot)) = \int\ p(f(\cdot) \mid f(\mathbf{z}) = \mathbf{u}) q(\mathbf{u}) \mathrm{d}\mathbf{u} \qquad (19)$$

When the pseudo-inputs z ∈ X M are defined as follows: q(u) ≈ p(u | y), which is an approximation of the posterior on u = f(z) ∈ RM. By conditioning process utilizing deterministic functions of process u = φ(f), this method can be further improved.

6. Results and discussion

The Windows 10 system requirements for development environment include 16 GB of RAM and an Intel(R) Core(TM) i5-1005G1 CPU. Jupyter VScode notebook. Visual Studio and Python are utilized in construction of suggested method. NLTK Python model is utilized for data preparation. Pandas and Keras are utilized to vectorise text. NumPy and pydata.org are utilized for data analysis as well as manipulation.

Dataset description- We made use of Global Forest Cover Change (GFC) data, which is available on GEE platform (version 1.8). In order to describe the global forest area and evolution from 2000 to 2020, it used global forest data from high-resolution Landsat TM satellite photography as well as offered a time series analysis of these images. The definition of tree cover for all vegetation types taller than five meters was canopy closure. Each of the seven files that make up each of the 10 × 10° tiles that make up the global dataset has a spatial resolution of roughly 30 m per pixel at equator. There were seven layers created in all, of which we will use first two: (1) the term "tree canopy cover" refers to canopy cover of all vegetation measured above five meters. It is encoded as a percentage output per grid cell ranging from 0 to 100. A threshold of 10% for tree cover was established. (2) The term "forest cover loss year" (lossyear) refers to the breakdown of total forest loss by detection year. It is encoded as 0 or a value between 1 and 20, signifying annual loss detected between 2001 and 2020.

In order to identify as well as map deforestation and forest degradation, utilized 1,465 Landsat Thematic Mapper (TM)/Enhanced Thematic Mapper (ETM+) pictures that were collected between 2000 and 2010 and covered the majority of the Brazilian Amazon Biome. Though occasionally photos with up to 30% cloud cover were included, vast majority of images had a maximum cloud cover of 20%. Annual area mapped varied from 106 to 157 photos, out of a maximum coverage of 192 for full research region, covering approximately 4 million km2, due to paucity of cloud-free Landsat images. Majority of absent sceneries originated from the study area's less populous and wetter areas. All years had good coverage of the southern and eastern Amazon, which experiences the great bulk of deforestation and forest degradation.

Moderate Resolution Imaging Spectroradiometer (MODIS) on NASA's Terra satellite provided us with LST and NDVI data. MODIS is supposedly positioned around 10.30 A.M. descending as well as 10:30 P.M. ascending equatorial crossing periods. As our first focus was on the years 2000–2005, we utilized MODIS Terra data instead of Aqua data. Product is a reprojection and averaging of MOD11B1 product. MOD11C1 product, which has a spatial resolution of 0.05° × 0.05°, is used in its production.

Table 1: Comparative for GFC dataset

Technique	Random accuracy	AUC	Mean precision	Normalized co-efficient	F1-score
LSTM	76	79	75	72	77
SVM	80	84	85	79	83
KPFRNN_VGEM	89	91	88	86	93

Table 2: Comparative for ETM+ dataset

Technique	Random accuracy	AUC	Mean precision	Normalized co-efficient	F1-score
LSTM	68	74	72	77	73
SVM	76	78	81	86	77
KPFRNN_VGEM	85	87	89	90	84

Table 3: Comparative for MODIS dataset

Technique	Random accuracy	AUC	Mean precision	Normalized co-efficient	F1-score
LSTM	84	75	78	79	89
SVM	88	85	86	84	91
KPFRNN_VGEM	98	95	94	97	93

Table-1-3 shows Comparative based on various smart grid security dataset. Dataset analysed are MIMIC-IV, ETM+ , MODIS dataset in terms of Random accuracy, AUC, mean precision, normalized co-efficient, F1-score.

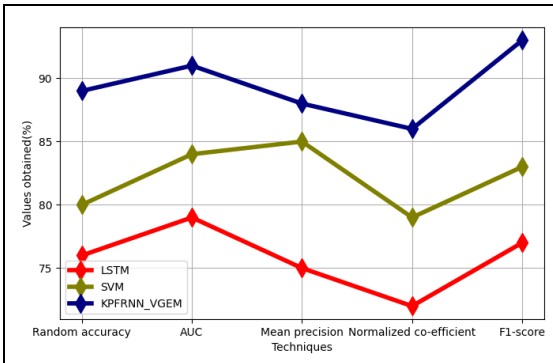

(a) GFC dataset

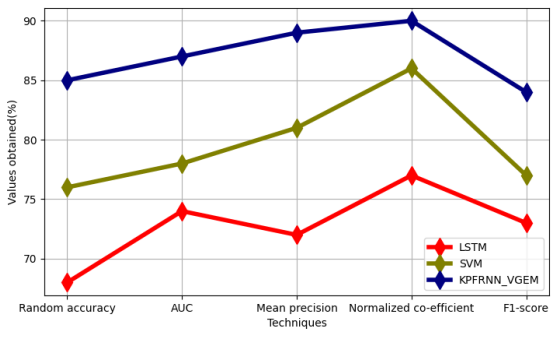

(b) ETM+

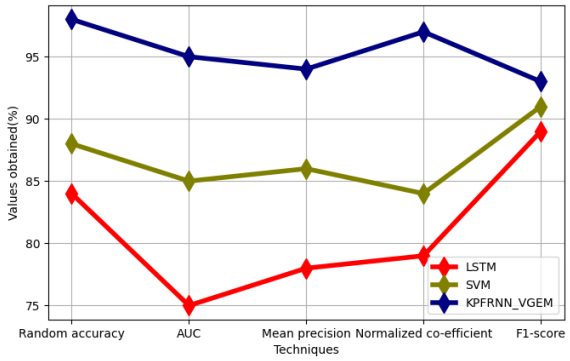

(c) MODIS dataset

Figure 2. (a)- (c) parametric analysis of existing LSTM for (a) MIMIC-IV, (b) ETM+ **, (c)** MODIS dataset

Fgure-2 (a) - (c) shows parametric analysis of existing LSTM in GFC dataset. For GFC dataset existing LSTM mean precision 75%, normalized co-efficient 72%, AUC 79%, random accuracy 76%, F1-score 73%. mean precision 72%, normalized co-efficient 77%, AUC 74%, random accuracy 68%, F1-score 73% for ETM+ ; existing LSTM mean precision 78%, normalized co-efficient 79%, AUC 75%, random accuracy 84%, F1-score 89% for MODIS dataset.

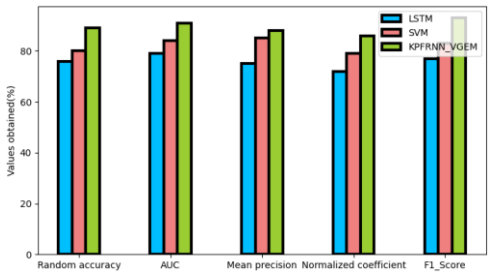

(a) GFC dataset

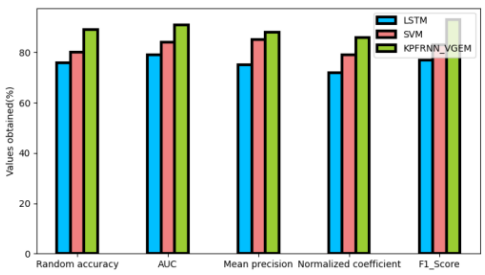

(b) ETM+

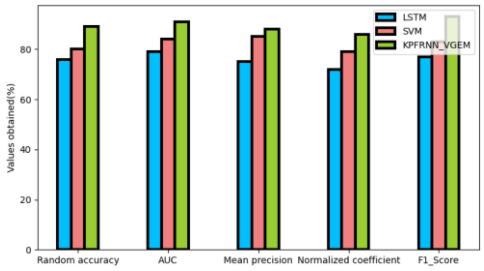

(c) MODIS dataset

Figure 3. (a)- (c) parametric analysis of existing SVM for (a) MIMIC-IV, (b) ETM+ , (c) MODIS dataset

Figure 3(a)–(c) shows parametric analysis of SVM in GFC dataset. SVM mean precision 85%, normalized co-efficient 79%, AUC 84%, random accuracy 80%, F1-score 83% on GFC dataset. For ETM+ , existing SVM achieved mean precision 81%, normalized co-efficient 86%, AUC 78%, random accuracy 76%, F1-score 77%; mean precision 86%, normalized co-efficient 84%, AUC 85%, random accuracy 88%, F1-score 91% for MODIS dataset.

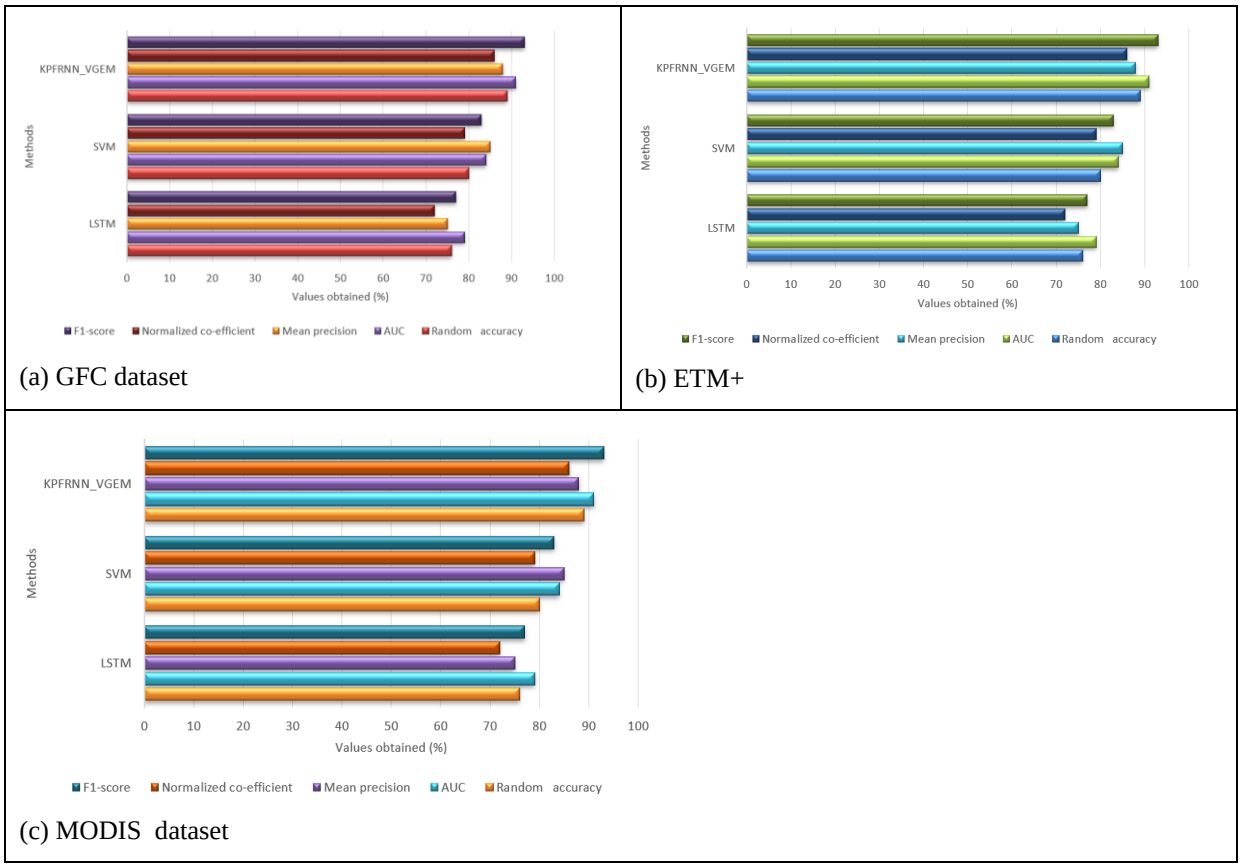

Figure 4. (a)- (c) parametric analysis of KPFRNN_VGEM for (a) MIMIC-IV, (b) ETM+ , (c) MODIS dataset

Parametric analysis of KPFRNN_VGEM in GFC dataset is displayed in above figure 4(a)–(c). KPFRNN_VGEM 88% mean precision, 86% normalized co-efficient, 91% AUC, 89% random accuracy, 93% F1-score for GFC dataset. For ETM+ , mean precision 89%, normalized co-efficient 90%, AUC 87%, random accuracy 85%, F1-score 84%. For MODIS dataset, mean precision 94%, normalized co-efficient 97%, AUC 95%, random accuracy 98%, F1-score 93%.

7. Conclusion

The main causes of the deterioration of urban thermal environment are changes in landscape and the LULCC brought about by urban growth and renewal. In order to model diversity of geographical regions, this study proposes a unique technique for temperature pattern analysis-based deforestation rate detection using machine learning. The suggested model gathers deforestation data based on temperature patterns and processes it for noise reduction and normalization. Then, using a variational Gaussian encoder markov model and a kernel principal fuzzy reinforcement neural network, the features of the data were retrieved and identified. Being a third-world nation, we have significant concerns about human-forest conflict and high population growth. Forest regions are particularly vulnerable to anthropogenic stress because of people's daily demands for commodities. The current forest sustainability can be led by deforestation probability zone analysis, daily monitoring, and appropriate management techniques. Primary goal of this study was to identify high-risk areas for deforestation and provide appropriate justifications for them, enabling the government to implement various management techniques. The outcomes of these machine-learning models will undoubtedly help policymakers manage forest resources sustainably while also preserving wild species and their habitats.

References

[1] R. Sun, F. Zhao, C. Huang, H. Huang, Z. Lu, P. Zhao, and R. Meng, "Integration of deep learning algorithms with a Bayesian method for improved characterization of tropical deforestation frontiers using Sentinel-1 SAR imagery," *Remote Sensing of Environment*, vol. 298, p. 113821, 2023.

[2] F. Dias, N. Suhadolnik, H. Camargo, and S. Da Silva, "Predicting the pulse of the Amazon: Machine learning insights into deforestation dynamics," *Journal of Environmental Management*, vol. 362, p. 121359, 2024.

[3] S. Srivastava and T. Ahmed, "DLCD: Deep learning-based change detection approach to monitor deforestation," *Signal, Image and Video Processing*, pp. 1-15, 2024.

[4] C. Singha, K. C. Swain, A. Moghimi, F. Foroughnia, and S. K. Swain, "Integrating geospatial, remote sensing, and machine learning for climate-induced forest fire susceptibility mapping in Similipal Tiger Reserve, India," *Forest Ecology and Management*, vol. 555, p. 121729, 2024.

[5] D. A. Subhahan and C. V. Kumar, "Deforestation rate estimation using crossbreed multilayer convolutional neural networks," *Multimedia Tools and Applications*, pp. 1-27, 2024.

[6] B. Haq, M. A. Jamshed, K. Ali, B. Kasi, S. Arshad, M. K. Kasi, and M. Ur-Rehman, "Tech-Driven Forest Conservation: Combating Deforestation With Internet of Things, Artificial Intelligence, and Remote Sensing," *IEEE Internet of Things Journal*, 2024.

[7] D. D. O. Maionchi, J. G. D. Silva, F. A. Balista, W. A. M. Junior, S. R. D. Paulo, I. J. D. Paulo, and M. S. Biudes, "Estimating hourly air temperature in an Amazon-Cerrado transitional forest in Brazil using Machine Learning regression models," *Theoretical and Applied Climatology*, vol. 155, no. 8, pp. 7827-7843, 2024.

[8] F. R. da Silva, S. F. Câmara, F. R. Pinto, F. J. da Costa, L. M. de Freitas, J. G. C. de Oliveira Júnior, and M. O. Soares, "Machine learning application to assess deforestation and wildfire levels in protected areas with tourism management," *Journal for Nature Conservation*, vol. 74, p. 126435, 2023.

[9] R. Manoharan, "Improving Security and Performance in Chaotic Optical Communication via Real-Time Pilot Signal Processing Techniques," *IETE Journal of Research*, pp. 1-9, 2025.

[10] M. Rajesh, S. Ramachandran, K. Vengatesan, S. S. Dhanabalan, and S. K. Nataraj, "Federated Learning for Personalized Recommendation in Securing Power Traces in Smart Grid Systems," in *IEEE Transactions on Consumer Electronics*, vol. 70, no. 1, pp. 88-95, Feb. 2024, doi: 10.1109/TCE.2024.3368087.

[11] B. Mishra, S. Panthi, S. Poudel, and B. R. Ghimire, "Forest fire pattern and vulnerability mapping using deep learning in Nepal," *Fire Ecology*, vol. 19, no. 1, p. 3, 2023.

[12] M. Zhang, A. A. Kafy, P. Xiao, S. Han, S. Zou, M. Saha, and S. Tan, "Impact of urban expansion on land surface temperature and carbon emissions using machine learning algorithms in Wuhan, China," *Urban Climate*, vol. 47, p. 101347, 2023.

[13] S. Ullah, M. Abbas, and X. Qiao, "Impact assessment of land-use alteration on land surface temperature in Kabul using machine learning algorithm," *Journal of Spatial Science*, pp. 1-23, 2024.

[14] J. Kang, B. Zhang, and A. Dang, "A novel geospatial machine learning approach to quantify non-linear effects of land use/land cover change (LULCC) on carbon dynamics," *International Journal of Applied Earth Observation and Geoinformation*, vol. 128, p. 103712, 2024.

[15] T. S. Arulananth, P. G. Kuppusamy, R. K. Ayyasamy, S. M. Alhashmi, M. Mahalakshmi, et al., "Semantic segmentation of urban environments: Leveraging U-Net deep learning model for cityscape image analysis," *PLOS ONE*, vol. 19, no. 4, p. e0300767, 2024. doi: 10.1371/journal.pone.0300767.